Research Article | Vol. 26, No. 18 | 3 Sep 2018 | OPTICS EXPRESS A892
Optics EXPRESS

Performance of a dielectric PVT concentrator for building-façade integration

ALBERTO RIVEROLA, ALEX MORENO, AND DANIEL CHEMISANA*

Applied Physics Section of the Environment Science Dept., University of Lleida, 25001 Lleida, Spain
**daniel.chemisana@macs.udl.cat*

Abstract: Concentrating photovoltaic-thermal (CPVT) systems, which can be integrated on buildings façades and use low-accuracy trackers and standard cells, have the potential to produce cost-effective electricity and heat. In this paper, a refractive cylindrical CPVT module with cells directly immersed in deionized water (DIW) or isopropyl alcohol (IPA) is designed, fabricated and experimentally tested. The interfaces between the cylinder and the fluids cavity have been optimized to maximize optical efficiency and irradiance uniformity, obtaining better results for a geometric concentration of 10x and IPA. The system achieves an optical efficiency of 81%, an acceptance angle of 1.07° and a non-uniformity coefficient of 0.13.

OCIS codes: (080.2740) Geometric optical design; (350.6050) Solar energy; (220.1770) Concentrators; (220.4298) Nonimaging optics; (040.5350) Photovoltaic.

References and links

1. EPBD, *Energy Performance of Buildings (EPBD) Directive 2010/31/EU* (European Parliament, 2010).
2. A. H. A. Al-Waeli, K. Sopian, H. A. Kazem, and M. T. Chaichan, "Photovoltaic/Thermal (PV/T) systems: Status and future prospects," Renew. Sustain. Energy Rev. **77**, 109–130 (2017).
3. R. M. da Silva and J. L. M. Fernandes, "Hybrid photovoltaic/thermal (PV/T) solar systems simulation with Simulink/Matlab," Sol. Energy **84**(12), 1985–1996 (2010).
4. D. Chemisana, "Building Integrated Concentrating Photovoltaics: A review," Renew. Sustain. Energy Rev. **15**(1), 603–611 (2011).
5. C. Lamnatou and D. Chemisana, "Concentrating solar systems: Life Cycle Assessment (LCA) and environmental issues," Renew. Sustain. Energy Rev. **78**, 916–932 (2017).
6. Y. Amanlou, T. Tavakoli, B. Ghobadian, G. Naja, and R. Mamat, "A comprehensive review of Uniform Solar Illumination at Low Concentration Photovoltaic (LCPV) Systems," Renew. Sustain. Energy Rev. **60**, 1430–1441 (2016).
7. S. Kurtz *Opportunities and Challenges for Development of a Mature Concentrating Photovoltaic Power Industry (Revision)* (2011).
8. A. Zacharopoulos, P. Eames, D. McLarnon, and B. Norton, "Linear Dielectric Non-Imaging Concentrating Covers For PV Integrated Building Facades," Sol. Energy **68**(5), 439–452 (2000).
9. N. Sarmah, B. S. Richards, and T. K. Mallick, "Evaluation and optimization of the optical performance of low-concentrating dielectric compound parabolic concentrator using ray-tracing methods," Appl. Opt. **50**(19), 3303–3310 (2011).
10. D. Freier, R. Ramirez-Iniguez, T. Jafry, F. Muhammad-Sukki, and C. Gamio, "A review of optical concentrators for portable solar photovoltaic systems for developing countries," Renew. Sustain. Energy Rev. **90**, 957–968 (2018).
11. S. P. Philipps, A. W. Bett, K. Horowitz, and S. Kurtz, "Current Status of Concentrator Photovoltaic (CPV) Technology," ISE/NREL Rep. (2015).
12. Y. A. Abrahamyan, V. I. Serago, V. M. Aroutiounian, I. D. Anisimova, V. I. Stafeev, G. G. Karamian, G. A. Martoyan, and A. A. Mouradyan, "The efficiency of solar cells immersed in liquid dielectrics," Sol. Energy Mater. Sol. Cells **73**(4), 367–375 (2002).
13. X. Han, Y. Wang, and L. Zhu, "Electrical and thermal performance of silicon concentrator solar cells immersed in dielectric liquids," Appl. Energy **88**(12), 4481–4489 (2011).
14. M. Vivar and V. Everett, "A review of optical and thermal transfer fluids used for optical adaptation or beam-splitting in concentrating solar systems," Prog. Photovolt. Res. Appl. **22**(6), 612–633 (2014).
15. D. Chemisana, E. F. Fernandez, A. Riverola, and A. Moreno, "Fluid-based spectrally selective filters for direct immersed PVT solar systems in building applications," Renew. Energy **123**, 267–272 (2018).
16. A. Riverola, A. Mellor, D. Alonso Alvarez, L. Ferre Llin, I. Guarracino, C. N. Markides, D. J. Paul, D. Chemisana, and N. Ekins-Daukes, "Mid-infrared emissivity of crystalline silicon solar cells," Sol. Energy Mater. Sol. Cells **174**, 607–615 (2018).
17. "SCHOTT catalog," http://www.schott.com.

#331849 https://doi.org/10.1364/OE.26.00A892
Journal © 2018 Received 16 May 2018; revised 25 Jul 2018; accepted 29 Jul 2018; published 21 Aug 2018

Optics EXPRESS

18. ASTM, "G173-03 Standard tables for reference solar spectral irradiances: direct normal and hemispherical on 37° tilted surface," B. Stand. **14.04**, (2004).
19. SAS Silicon cells, "SR6SKUN 156.75 x 156.75 Monocrystalline Solar Cell 5 Bus bars," (2017).
20. F. Duerr, Y. Meuret, and H. Thienpont, "Tailored free-form optics with movement to integrate tracking in concentrating photovoltaics," Opt. Express **21**(S3 Suppl 3), A401–A411 (2013).
21. E. Muslimov, E. Hugot, W. Jahn, S. Vives, M. Ferrari, B. Chambion, D. Henry, and C. Gaschet, "Combining freeform optics and curved detectors for wide field imaging: a polynomial approach over squared aperture," Opt. Express **25**(13), 14598–14610 (2017).
22. A. Mellor, J. L. Domenech-Garret, D. Chemisana, and J. I. Rosell, "A two-dimensional finite element model of front surface current flow in cells under non-uniform, concentrated illumination," Sol. Energy **83**(9), 1459–1465 (2009).
23. D. Chemisana and J. I. Rosell, "Electrical performance increase of concentrator solar cells under Gaussian temperature profiles," Prog. Photovolt. Res. Appl. **21**, 444–455 (2013).
24. H. Baig, K. C. Heasman, and T. K. Mallick, "Non-uniform illumination in concentrating solar cells," Renew. Sustain. Energy Rev. **16**(8), 5890–5909 (2012).
25. M. Victoria, C. Domínguez, I. Antón, and G. Sala, "Comparative analysis of different secondary optical elements for aspheric primary lenses," Opt. Express **17**(8), 6487–6492 (2009).
26. A. Moradi, E. Sani, M. Simonetti, F. Francini, E. Chiavazzo, and P. Asinari, "CFD modeling of solar collector with nano-fluid direct absorption for civil application," Proc. 3rd Ed. Int. Conf. Microgeneration Relat. Technol. (2013).
27. S. Eiternick, K. Kaufmann, J. Schneider, and M. Turek, "Loss Analysis for Laser Separated Solar Cells," Energy Procedia **55**, 326–330 (2014).

1. Introduction

Building-integrated solar energy systems are positioned as an advantageous option not only to meet the European Union requirements regarding nearly-zero energy buildings [1], but also to address the goal of generating energy in an efficient and green way. Among them, hybrid photovoltaic-thermal (PVT) collectors stand out due to their on-site cogeneration of electricity and heat with global efficiencies around 70% (electrical near 20% and thermal higher than 50%) [2]. In the frame of building-integrated solar systems, space availability is one of the most limiting factors. This may be overcome by PVT collectors since it has been demonstrated that 60% additional area is required for a separate solar thermal collector and PV module to produce the same yield as a PVT liquid system [3].

Concentrating photovoltaics (CPVs) allow making a more cost-effective system considering that expensive solar cell material is partly replaced by lower cost optical elements. In addition, the environmental impact and the efficiency are enhanced under concentrated illumination [4,5]. Low-concentration modules ease building integration applications, in particular cylindrical optical systems whose solar tracking is less restrictive than in high CPV (HCPV) (single-axis instead of two-axis) and also standard crystalline silicon (c-Si) solar cells may be utilized [4,6–10]. At present, the utilization of standard c-Si PV modules represents an important advantage in comparison to HCPV cells. This relies on several factors: (i) HCPV modules are only competitive for high direct normal irradiance (DNI) locations (above 2000 kWh/m^{2}year); (ii) Levelized cost of electricity of HCPV is expected to equal the one of c-Si in around 2025 considering direct normal irradiances of 2000 kWh/m^{2}year in the case HCPVs and global horizontal irradiances of 2000 kWh/m^{2}year in the case of c-Si PVs [11].

Direct-immersed PVs and CPVs have proved to enhance efficiency in response to a reduction of the Fresnel losses respect to a bare PV, a reduction of the surface recombination losses and a better temperature control by the reduction or elimination of the thermal contact resistance at the interface between PVs and dissipater [12,13]. By merging the positive characteristics of PVTs with those of direct-immersed PVs or CPVs, direct-immersed CPVT collectors are obtained. The concept of direct-immersed CPVT modules with circulating dielectric liquids was commenced in the late 70's based on static reflective concentrators. Afterwards, the approach was not actively pursued for 20 years. In the last decade, an increased interest in developing new direct-immersed CPV and CPVTs is observed. However, this type of systems should be further studied for building integration applications [14,15].

Optics EXPRESS

The present research aims at developing an innovative direct-immersed PVT concentrator for building integration. For that purpose, the system design is first introduced. Later, the concentrator is optimized and analyzed by ray-tracing. The optimal options derived from the theoretical results are fabricated and experimentally assessed. Finally, the main conclusions are stated.

2. System design

The system designed is composed by a cylindrical case and an inner cavity filled with the circulating dielectric liquid in which the cells are immersed (see detail of Fig. 1). The module tracks the solar altitude angle variation in a relatively simple way by rotation, which can be driven by a single motor and thus facilitates building integration. The solar movement along the azimuthal direction remains untracked taking benefit from the linear concentration (the system has optical power only in one plane -perpendicular to the cylinder axis-) and assuming that the cylinder axis lies along the east–west direction. The modules are designed to be placed south-oriented (Northern Hemisphere) in rows as an array so that the appearance is similar to ordinary blinds and can produce useful energy to cope with building demands. A secondary movement has been foreseen to control the vertical distance between modules to ensure no shading between them. This movement also allows controlling the interior illumination depending on the user's requirements to prioritize daylighting or energy production. Figure 1 shows an architectural image obtained by rendering the optical design developed superimposed onto a window. The vertical distance between individual concentrators is set to the minimum which avoids shading between modules and prevents from direct irradiance to enter inside the building (illumination control). Clear difference in the lighting is appreciated in comparison to the right window where only a standard glazing is incorporated. In the detail of the concentrator, its main features are indicated. In addition, it can be appreciated the functionality of the concentrating system as see-trough glazing.

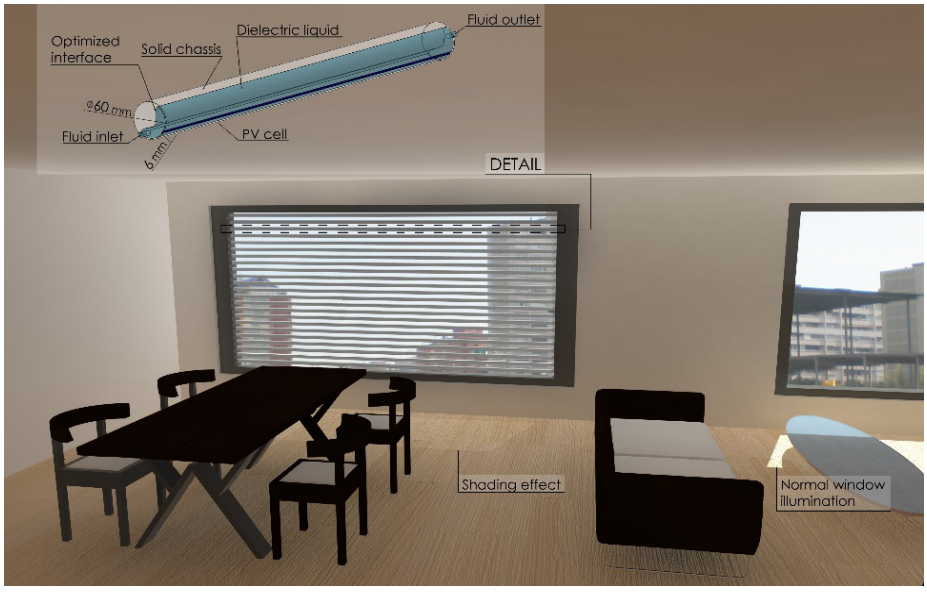

Fig. 1. Architectural image of the concentrating system incorporated on the left window. The shading and the see-through effect of the system can be appreciated together with a 3D detail of a module with its main characteristics. Differential lighting is illustrated by incorporating a standard glass pane on the right glazing.

The system has been optically modelled and optimized to maximize the convergence of incident solar rays towards the PV cell while producing a uniform illumination pattern. A full

ray-tracing algorithm which assesses the rays' path, the optical transitions at each system interface, the absorption travelling through the different media and the PV surface reflection has been developed determining the amount of incident power reaching the PV cell. The code computes at each interface the amount of power which is transmitted by the Fresnel coefficients as a function of the incident angle, the wavelength and the corresponding optical constants. The absorption at each medium has been computed according to Beer-Lambert law, which depends on the extinction coefficient of every material and the ray's path through the corresponding medium. The absorption of the solar cell is also considered for rays reaching the target. With this regard, the model developed by Riverola et al. has been utilized [16].

The cylindrical tube has an outer diameter of 60 millimeters and it is considered to be borosilicate glass (BK7). This glass is widely used for precision lenses due to its good optical, thermal and mechanical properties and its resistance to chemical and environmental damages. Other candidates such as acrylics can suffer degradation exposed to some dielectrics as, for instance, alcohols. In addition, their optical characteristics for the model inputs present wider variability (especially in the extinction coefficient) whereas for BK7 are well defined and reported in the literature [17]. Two dielectric liquids to immerse the cell have been selected: deionized water (DIW) and isopropyl alcohol (IPA). Both candidates have a great heat extraction capacity and weak absorption at frequencies in which solar cells are able to generate electricity. These two and other dielectric liquids were widely studied in the literature in terms of electrical and thermal properties, stability and operational conditions and DIW and IPA, or a mixture of them, were shown to be suitable candidates for PVT applications [15]. In addition, the dielectric liquids selected were assessed under the operational temperature range estimated for the solar collector (15 - 50 °C) and no variations in the electrical insulation properties were observed since the PV cell efficiency was not reduced in a higher percentage than that associated to the temperature increase. Both dielectric liquids present high electrical insulation characteristics for the present application and although the dielectric properties of both liquids vary slightly with temperature, these variations do not affect PV cell performance.

Typically, low-medium concentration systems try to use standard PV technologies and low-accuracy trackers resulting in geometric concentrations ranging from 10x to 20x [7]. Three different cell sizes have been studied 3, 4 and 6 millimeters which result in three different geometric concentration ratios (quotient between the aperture area of the concentrator and the PV cell surface) 20x, 15x and 10x respectively given that the aperture is 60 millimeters. The concentrations interval selected balances the benefits of CPV and the techno-economical features related to the use of standard PV cells and low-accuracy trackers. This is aligned with what is reported in [7]. Concentrations higher than 20x were not considered so that standard silicon solar cells may be utilized with negligible impact on the series resistance. In addition, cells higher than 6 millimeters would limit the amount of diffuse light entering through the system which is key to ease its building integration on windows. The cell has been positioned atop of a tube with a radius of 28 millimeters which serves to confine the dielectric liquid.

Incident rays were assumed to face the concentrator perpendicularly (solar altitude tracking and at solar noon) taking into account the natural sun beam aperture (semiangle of 4.65 mrad). The spectral distribution of energy was set to be the standard ASTM G173-0.3 AM1.5D spectrum [18] and the spectral cell response was taken from the commercial mono-crystalline silicon cells from SAS that will be used in the prototype fabrication [19].

In the frame of the optimization, the interface between the BK7 and the dielectric liquid has been set as a free-form profile. Free-form geometries are most commonly modelled using Bezier splines, B-Splines or NURBS [20,21]. In this paper, the free-form profile has been modelled as a B-Spline curve with N control points which allows tailoring the geometry to the specific application. In order to find the best interface geometry for every liquid and

Optics EXPRESS

geometric concentration ratio, an optimization based on a genetic algorithm has been performed. The variable to modify in the optimization was selected to be the height (y-coordinate) of the N control points of the free-form line. Several constraints were incorporated to limit the search space and consequently the optimization time. Control points regarding x-coordinate were evenly distributed into the concentrator aperture width and fixed. Values of N ranging from 20 to 80 were tested showing that 40 control points were sufficient to provide enough freedom while keeping the optimization time bearable. A merit function with two objectives was defined. The first objective is the current produced by the PV cell should be as high as possible. Therefore, the optimization must tailor the chassis-liquid interface to reduce the Fresnel losses between the BK7 and the dielectric liquid, to obtain the optical paths through all the mediums so that the spectral absorption at wavelengths where the cell is able to produce electricity is reduced and to focus the rays towards the cell. In addition, the angle of incidence over the cell influences the absorptivity and therefore high angles of incidence are not desired. The second objective is to have a uniform spatial illumination over the cell. The lack of irradiance uniformity over the cell reduces the fill factor, the efficiency and the open circuit voltage. Different internal currents which flow from highly to weakly illuminated domains have a significant impact on the power output. Also, it causes thermal stress, which can considerably impact the long-term reliability [22–24]. The non-uniformity has been computed by the next equation [Eq. (1)] where $J_{sc,x}$ is the local short-circuit current density over the cell:

$$U = \frac{\max\left(J_{sc,x}\right) - \min\left(J_{sc,x}\right)}{\max\left(J_{sc,x}\right) + \min\left(J_{sc,x}\right)} \tag{1}$$

Both objectives were considered into a function of weights [Eq. (2)], each one with its corresponding relative weight. $J_{sc,\eta\,=\,1}$ is defined as the global short-circuit current density obtained for an optical efficiency (η) of 1, J_{sc} is the global short-circuit current density and w_1 and w_2 are the corresponding weights. The optical efficiency is defined for the Si PV spectral response bandwidth and is calculated by the quotient between the incident power at the aperture of the concentrator and the power received on the PV cell area.

$$W = w_1 * \frac{\left|J_{sc,\eta=1} - J_{sc}\right|}{J_{sc,\eta=1}} + w_2 * U \tag{2}$$

The optimization has been conducted for a solar azimuth angle (ϕ) equal to 0° (at solar noon) since under this condition the maximum irradiance at the concentrator aperture plane is achieved. On the other hand, optimized profiles have been determined for other solar azimuth angles of incidence but daily mean optical efficiencies obtained (for ϕ ranging from −90° to 90°) are always higher for the optimized profiles under ϕ = 0° in both configurations, DIW and IPA. The optical performance variation as a function of the azimuth is analyzed in section 3.

3. Ray-tracing characterization

From the optimization, the best interface curve for each dielectric liquid and concentration has been found, resulting in six different profiles. Table 1 shows the main properties for each configuration. Cavities filled with IPA achieve higher maximum optical efficiencies (ϕ = 0°) of 80-81% depending on the geometric concentration whereas using DIW, the optical efficiency is limited to 75-76% due to a higher absorption in the liquid. Good irradiance uniformity (U < 0.2) is obtained in all the systems with DIW while in the case of IPA and for geometric concentrations higher than 15x a convex Gaussian-like shape is observed on the

Optics EXPRESS

irradiance profile resulting in a worse irradiance distribution (U ≈0.4). The acceptance angle is defined by the misalignment angle for which the optical efficiency drops 10% relative to the maximum. In the systems studied here, the misalignment angle varies from ± 1.11° for the lowest concentration to ± 0.4° for the highest. Systems filled with DIW obtain slightly higher acceptance angles. The effective concentration is formulated as the product of the geometric concentration and the optical efficiency.

From the results, it can be seen that increasing the geometric concentration leads to reduced acceptance angles but also uniformity and efficiency have small detrimental impacts. The acceptance angle is directly related to the cost of kWh of electricity produced since lower acceptance angles result in a more expensive tracking [25]. For the present application and using DIW, configurations with geometric concentrations between 10x and 15x are better suited due to high optical efficiencies and high irradiance uniformity together with bearable tracking requirements. In the case of IPA, the irradiance non-uniformity factor and the acceptance angle are remarkably affected by geometric concentrations higher than 10x, being this configuration selected as the optimum one. The ray-tracing plots of the optimum profiles for 10x are depicted in Fig. 2. From here on, although the configuration with DIW presents a range of optimal concentrations from 10x to 15x, 10x is selected in both cases for a better comparison since the optimum concentration with IPA is 10x.

Table 1. Optimization results

Magnitude	DIW			IPA		
Geometric concentration (-)	10	15	20	10	15	20
Maximum optical efficiency (-)	0.76	0.76	0.75	0.81	0.81	0.80
Maximum effective concentration (suns)	7.6	11.4	15.0	8.1	12.1	16.0
Non-uniformity (-)	0.14	0.19	0.20	0.13	0.40	0.41
Acceptance angle ± (°)	1.11	0.71	0.47	1.08	0.53	0.40

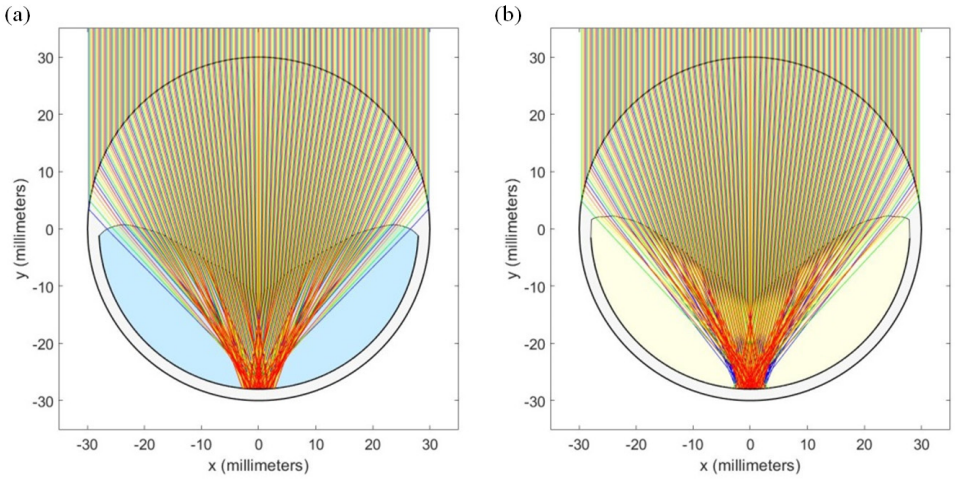

Fig. 2. Ray-tracing of the optimum interfaces at 10x for (a) DIW and (b) IPA. Four wavelengths are depicted from 400 to 1100 nm.

The irradiance profiles over the cell for both dielectric liquids optimal configurations at 10x are plotted in Fig. 3 (a), showing uniform trends around an effective concentration of 8 suns. For DIW, the maximum concentration is 8.7 suns with an average of 7.6 suns while for IPA the maximum is 8.8 suns with an average of 8.1 suns. Looking at Fig. 3 (b), the relative efficiency as a function of the misalignment angle can be seen. The relative efficiency decreases linearly with increasing misalignment angles. Since the system is designed for building integration purposes (potentially substituting window blinds), this allows for an

Optics EXPRESS

effective mechanism to control the amount of light entering into the building. Based on the linear performance of the efficiency reduction, both designs preserve optical efficiencies above 50% for misalignment angle of ± 4°.

The optical losses that affect the optical efficiency are disaggregated to better identify the phenomena or the elements that cause them. Five energy losses in the proposed design arise: (1) Fresnel losses at the air-BK7 interface, (2) absorption in the BK7, (3) Fresnel losses at the BK7-liquid interface, (4) absorption in the liquid and (5) reflection at the solar cell (considering that there is no transmission through the cell given its fully metallized rear surface). Table 2 shows the individual optical efficiency values obtained after each optical loss (global optical efficiency may be calculated by the product of the individual efficiencies) for the two liquids and for a concentration of 10x (similar values are obtained for 15x with DIW). Since the outer cylindrical shape of the system is the same for both dielectrics, the Fresnel losses associated with the air-BK7 interface are the same (Fresnel 1). The BK7 absorption also results similar even if the optical path lengths through the glass are not equal, the absorption is weak and results in nearly the same values. Concerning the transmission from the glass to the dielectric, the efficiency is slightly higher for IPA since the refractive index of IPA is higher than the one of DIW and therefore closer to BK7. The main difference relies on the dielectric liquid absorption where the DIW is 5.5% more absorptive than IPA. Concerning the last loss mechanism, reflection at the solar cell, both obtain similar values.

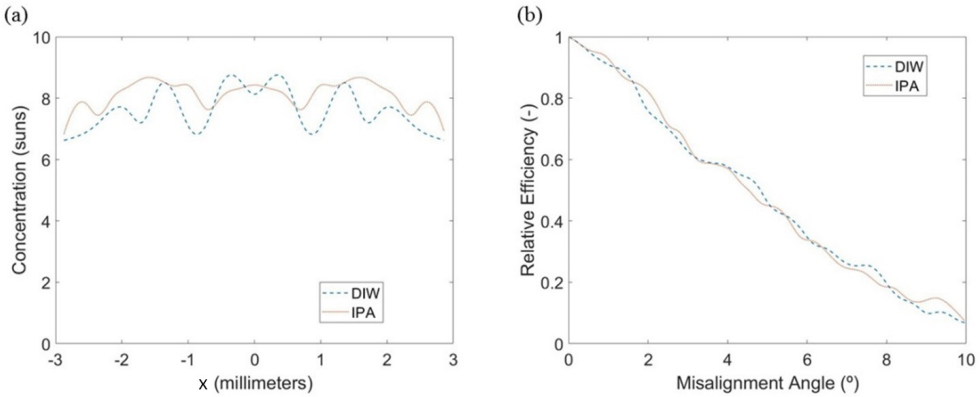

Fig. 3. (a) Solar concentration over the solar cell for a geometric concentration of 10x for both dielectric liquids (DIW and IPA). (b) Relative efficiency vs. Misalignment angle for a geometric concentration of 10x for both dielectric liquids (DIW and IPA).

Table 2. Detailed Optical Losses under 10x

	DIW	IPA
Optical Loss	**Optical Efficiency (%)**	
Fresnel 1	92.9	92.9
BK7 abs.	99.5	99.5
Fresnel 2	98.7	99.0
Liquid abs.	86.5	92.0
Reflected cell	96.0	95.9

The spectral optical efficiencies for both systems together with the spectral short-circuit current density ($J_{sc}(\lambda)$) have been plotted in Fig. 4 to better explain the differences between both systems. The $J_{sc}(\lambda)$ comprises the bandwidth obtained by considering the AM1.5D spectrum jointly with the Si spectral response and indicates the region where the optical efficiency should be maximum. Out of this region, the optical efficiency should be minimal since these photons don't contribute to electrical generation and should be absorbed by the liquid in order to prevent from heating the cell up. The spectral optical absorption of the two dielectric liquids, which is directly related to its corresponding extinction coefficient, is

Optics EXPRESS

noticeable different and shapes the areas in Fig. 4. DIW presents a higher extinction coefficient than IPA for wavelengths higher than 900 nm resulting in an increasing absorption for growing wavelengths. It can be appreciated that from 900 nm to 1100 nm the configuration with IPA surpasses clearly the one with DIW. Therefore, the system with IPA is better as an electricity generator but, from the thermal point of view, DIW shows greater capabilities since it absorbs photons with wavelengths larger than 1200 nm which otherwise would heat the cell up and it has better thermal properties as higher specific heat capacity [15].

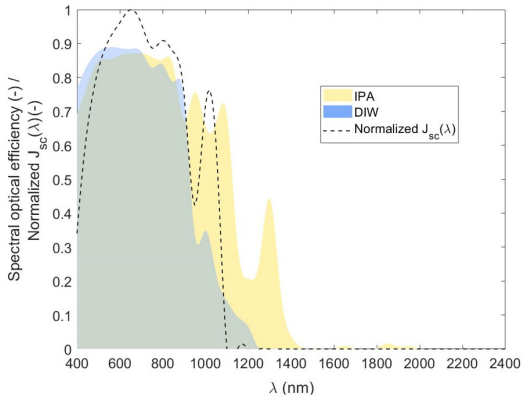

Fig. 4. Spectral optical efficiency for DIW and IPA at 10x together with the normalized spectral short-circuit current ($J_{sc}(\lambda)$) (black dashed line) to highlight wavelengths at which the spectral optical efficiency should be maximum.

Finally, as indicated at the end of Section 2, the system optical performance variation due to the untracked solar azimuth angle (ϕ) should be considered to completely characterize the system. Figures 5 (a) and (b) show the rays' optical efficiency as a function of ϕ and the rays' initial x-coordinate for both systems at 10x. In this way, it is possible to discern where the systems are more efficient and how it changes as the azimuth angle increases. Both systems present higher optical efficiencies close to the center of the cylinder since incidence angles are lower and thus the initial Fresnel losses. On the other hand, the rays' efficiency decreases sharply for the marginal (extreme) rays (greater incident angles leading to higher Fresnel losses). As ϕ increases, in addition to shortening the convergence distance due to field curvature aberration, Fresnel losses and absorption (larger path lengths) get augmented reducing the rays' efficiency. Marginal rays start missing the target from $\phi \approx 30°$ on both systems (dark blue area in Figs. 5 (a) and (b)) by a combination of Fresnel losses (reflection) and total internal reflection (TIR). TIR begins for the marginal rays at $\phi \approx 40°$ and the critical ϕ increases sequentially for rays approaching the center up to $x \approx \pm 5°$, from where the TIR effect is not produced anymore. It should be noted that TIR condition changes slightly as a function of wavelength since the refractive index is wavelength dependent. On the other hand, the central rays reach the cell up to $\phi \approx 55°$ for DIW and $\phi \approx 60°$ for IPA. Then, these rays miss the target due to the strong field curvature (only the central ray reaches the cell). Figure 5 (c) illustrates these effects for $\phi = 60°$ and at 589.3 nm (mean sodium D-lines) in the configuration with DIW (the case with IPA is analogous). Monochromatic modelling at a characteristic wavelength has been conducted to obtain a clearer ray-tracing plot. It can be appreciated that near the center, in a zone of about ± 8 mm, rays are refracted but, except the central ray, fall out of the cell. The other rays, indicated by dashed lines, undergo TIR. Integrating the rays' efficiency along the x-axis for every azimuth angle, the system overall efficiency is derived and plotted in Fig. 5 (d). It can be seen that the system with IPA is more efficient for $\phi = 0°$ (as it was shown previously) and also has better azimuth acceptance. The

Optics EXPRESS

system with DIW achieves an optical efficiency of 76% at $\phi = 0°$ to be compared with 74% at $\phi = 25°$ and 45% at $\phi = 45°$ while the one with IPA presents an optical efficiency of 81% at $\phi = 0°$ to be compared with 80% at $\phi = 25°$ and 51% at $\phi = 45°$. Based on the azimuth optical efficiency response, the design with IPA results in a better performance by maintaining high optical efficiencies for a wider angular range.

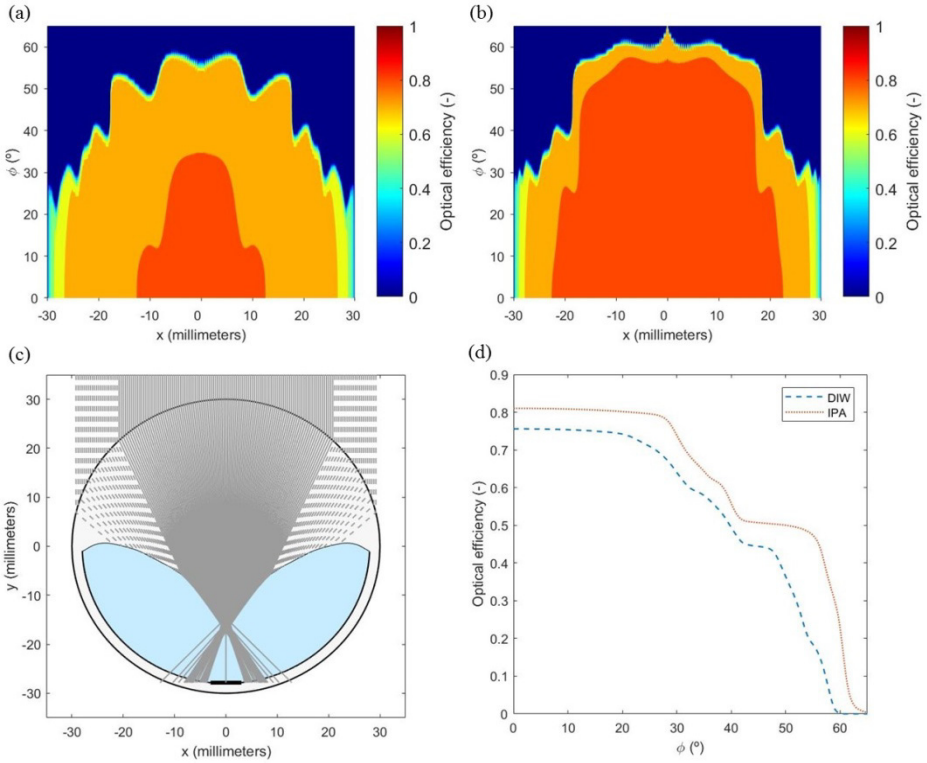

Fig. 5. Optical efficiencies as a function of the initial rays x-coordinate and the solar azimuth angle for DIW (a) and IPA (b) with solar altitude tracking. (c) Ray-tracing for $\phi = 60°$ and at 589.3 nm (mean of sodium D-lines) in the configuration of 10x with DIW - dashed lines indicate that these rays are under TIR. (d) Overall system efficiencies as a function of azimuth angle for DIW and IPA.

4. Fabrication and experimental optical performance

Prototypes of the concentrators with an optical aperture width of 60 mm and geometric concentration of 10x were fabricated to validate the optical design and to analyze the performance of the PV cell. PMMA was selected to demonstrate performance prior to the final manufacturing with BK7 (more resistant to alcohols -IPA- and with higher optical performance) since from the mechanical processing point of view is friendlier than optical glasses. This fact allowed that all the fabrication and associated improvements were conducted in the laboratory of the research group. The lens inner profile was obtained by CNC machining and polishing processes. Nonetheless, the optical properties of PMMA are different from BK7 and optimizations for both dielectric liquids and PMMA were conducted to obtain its corresponding interface profiles which vary slightly with respect to BK7. However, since the transmittance of both materials for the Si PV sensitivity bandwidth (300 nm-1100 nm) is analogous [26] and the Fresnel losses do not change to a great extent (<0.5%), the optical efficiency in the frame of the PV generator of both systems remains almost equal (DIW + PMMA = 0.76 & IPA + PMMA = 0.80). Figure 6 shows the mechanized lens for the case of DIW (a) jointly with the assembled prototype (b) where the

Optics EXPRESS

concentrated beam over the cell can be distinguished. In Fig. 6 (c), a detail of the lens without the dielectric liquid and illuminated with a divergent point light source is included to qualitatively illustrate optical performance.

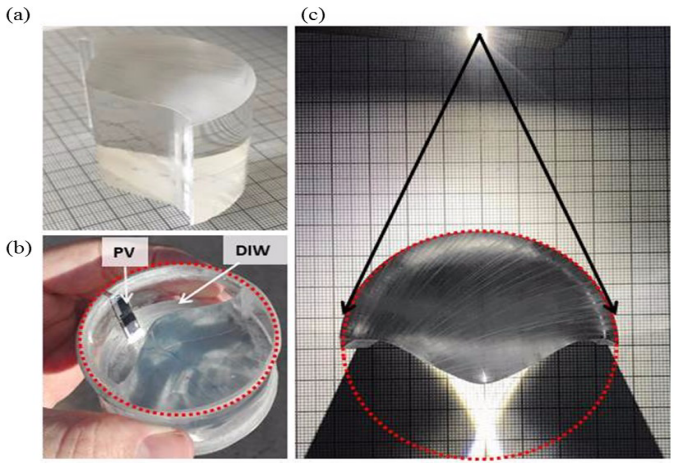

Fig. 6. (a) Mechanized lens for the case of DIW. (b) Prototype where the concentrated beam over the cell can be seen. (c) Detail of the lens without the dielectric liquid and illuminated with a divergent point light source to qualitatively illustrate optical performance.

By means of a diode laser (CrystaLaser, λ = 640.1 nm), the optical designs have been validated by comparing the widths of the simulated concentration profiles at the same wavelength with the experimental widths measured placing a millimeter paper at the cell plane. Figure 7 shows the modelled concentrated profiles together with a photo of the laser concentrated spot measured on the millimeter paper. Good agreement between modelled and experimental spot sizes is observed for both designs, with relative errors lower than 1%.

The PV cells incorporated in the prototypes are commercial mono-crystalline silicon cells from SAS, as indicated in Section 2, and were adapted to the required width (6 mm) by Nd:YAG laser cutting. The main electrical parameters under standard test conditions after the cutting process are: open circuit voltage (V_{oc}) = 0.609 V, J_{sc} = 38.3 mAcm^{-2}, fill factor (FF) = 70.2% and electrical efficiency (η_e) = 16.4%. It should be noted that detrimental impacts on the V_{oc} and the FF were observed compared to the original cell. These effects are attributed to a reduction of the parallel resistance due to edge shunts and higher recombination [27]. On the contrary, shunts do not affect the J_{sc} values and thus the characterization of the experimental optical concentration by the ratio between short-circuit currents is allowed.

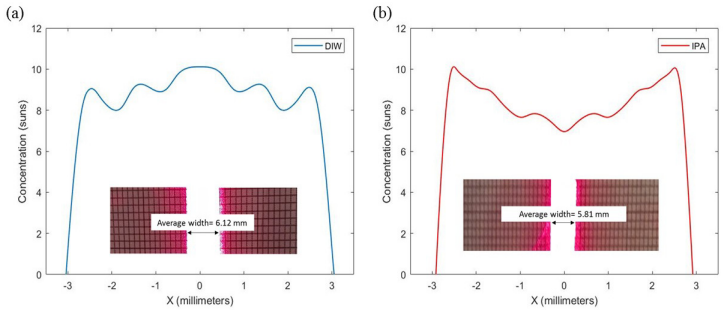

Fig. 7. Simulated uniformity profile for λ = 640.1 nm and validation by comparing the profiles widths with a millimeter paper on the cell plane (details incorporated on the graphs) for DIW (a) and IPA (b).

Optics EXPRESS

The prototypes were placed onto a two-axis tracker outdoors which was equipped with a pyranometer (Kipp&Zonen CMP 6) and a pyrheliometer (Kipp&Zonen CHP1) to measure the global and direct normal irradiances. The cells had attached a T-type thermocouple to its rear surface to register operation temperatures. Furthermore, the *J-V* characteristic curve was traced by the Keithley 2460 sourcemeter. Figure 8 shows the experimental *J-V* curve for both modules under a global irradiance of 1043 Wm^{-2} and a direct normal irradiance of 932 Wm^{-2}. The temperatures were controlled and kept as close to 25°C as possible, resulting in 26.4°C for DIW and 26.8°C for IPA.

The experimental optical efficiency can be derived from the *J-V* curve and the aforementioned electrical data by comparing the short-circuit current densities. The optical efficiency for DIW is 73.5% and for IPA 76.5%. The difference with the theoretical results is attributed to manufacturing inaccuracies. In addition, the *FF* remains almost constant for IPA being 70.1% and for DIW is somewhat reduced but still close to the bare PV (67.5%).

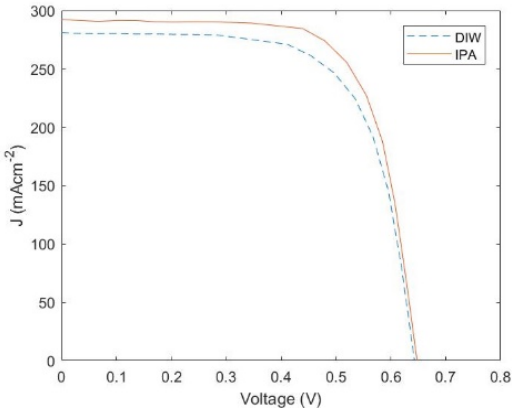

Fig. 8. Experimental current density-voltage characteristic of the system with DIW and IPA for a global irradiance of 1043 Wm^{-2}.

5. Conclusion

Two innovative cylindrical low-concentration photovoltaic systems with the cells directly immersed in dielectric liquids (deionized water, DIW, and isopropyl alcohol, IPA), for building integration purposes, have been designed and optimized. The system is based on a cylindrical BK7 chassis which confines the dielectric liquids. The interfaces between the BK7 and the dielectrics have been optimized for three different geometric concentrations (10x, 15x, and 20x), obtaining better results from 10x to 15x for DIW and for 10x with IPA. The system with DIW achieves an optical efficiency of 76%, with a misalignment acceptance angle from 1.11° (10x) to 0.71° (15x) and a non-uniformity coefficient from 0.14 (10x) to 0.19 (15x). On the other hand, in the case of IPA the system optical efficiency is enhanced (81%), the acceptance angle to misalignment is 1.07° and the non-uniformity 0.13. The designs' performances for angular variations in the direction along the cylinder axis (non-tracked direction) have been analyzed. Results indicate an adequate performance for the both systems, achieving an angular zone of 50° (± 25°) where optical efficiencies are kept around its maximum value. For wider angular variations, the device containing IPA preserves efficiencies at slightly higher values, reaching mean efficiencies over 50% for an angular range of 90° (± 45°). Based on the achieved results the design configuration with the optimized cavity filled with IPA is positioned as the best option.

Initial prototypes were fabricated and experimentally investigated which validated the optical model developed and demonstrated feasibility of the design. The refractive system

Optics EXPRESS

proposed shows potential to be cost-effective due to the use of standard silicon solar cells and low-accuracy trackers to partially cover electricity and heat energy demands of buildings.

Funding

Ministerio de Economía y Competitividad (MINECO) (ENE2013-48325-R, ENE2016-81040-R BES-2014-069596); Generalitat de Catalunya (2017FI_B_01171, 2017 SGR 1276).